Quasicrystal and approximant structures in the Al - Cu - Fe system

1996 J. Phys.: Condens. Matter 8 2487

(http://iopscience.iop.org/0953-8984/8/15/002)

J. Phys.: Condens. Matter **8** (1996) 2487–2512. Printed in the UK

Quasicrystal and approximant structures in the Al–Cu–Fe system

M Quiquandon†, A Quivy†, J Devaud†, F Faudot†, S Lefebvre‡, M Bessière‡ and Y Calvayrac†

† CECM/CNRS, 15 rue G Urbain, F-94407 Vitry Cédex, France

‡ LURE/CNRS/CEA/MEN, Bâtiment 209d, F-91405 Orsay Cédex, France

Received 21 September 1995, in final form 27 November 1995

Abstract. We present an extensive study of the approximant phases present in the Al–Cu–Fe phase diagram in the vicinity of the icosahedral phase. In addition to the rhombohedral and the two pentagonal phases previously observed, a new orthorhombic approximant has been identified. The identification of these structures, via x-ray diffraction and TEM, is based on both symmetry considerations and the 'shear' description in the perpendicular space. These simple geometric tools give very satisfactory and accurate crystallographic results. This suggests that these phases derive from the parent icosahedral phase both via systematic introduction of atomic jumps preserving most of the atomic local environments and via long-range atomic diffusion.

1. Introduction

The goal of this paper is to present a synthesis of work on the phase diagram of the Al–Cu–Fe system together with a method of characterizing the crystallography of the approximant phases by x-ray diffraction techniques.

The ternary system Al–Cu–Fe has aroused great interest since the discovery of a quasicrystalline icosahedral phase by Tsai *et al* [1]; this was initially located as regards composition in the vicinity of $Al_{65}Cu_{20}Fe_{15}$. Several authors have determined the ternary phase diagram around this composition [2–5]. Closely related phases called 'approximant' phases that are in competition with the icosahedral phase have been observed. In addition to the already known rhombohedral and pentagonal phases [6–14] we have characterized a new orthorhombic phase and determined the equilibrium phases at 700 °C.

Approximant phases—which turn out to be periodic in general—share many structural and physical properties with their parent high-symmetry quasicrystal: most of the transport properties measured for the icosahedral phases are shared by their approximants [15–19]; this makes plausible the hypothesis that approximant phases have essentially the same short- and medium-range order—up to several nanometres—as the parent quasicrystal. We will designate as an approximant structure, or simply an approximant, any structure—not necessarily periodic—whose diffraction pattern is close, as regards peak locations and intensities, to that of the parent high-symmetry quasicrystal (see [20] for a general discussion).

The paper is divided into four main sections.

Section 1 discusses the experimental conditions including alloy preparation, thermal treatments and characterization techniques (differential thermal analysis, x-ray and electron diffraction) that have been used to establish the equilibrium phase diagram.

0953-8984/96/152487+26$19.50

Section 2 discusses the geometric tool used to determine the various approximants from the diffraction data based on the 'shear' method as initially proposed by Jarić and Qiu [21].

Section 3 discusses the equilibrium phase diagram around the icosahedral phase region, and the structures of the observed approximants.

Section 4 is a general conclusion to the work.

2. Experimental conditions and diffraction pattern indexing

2.1. Experimental details

The alloys were prepared from the pure elements (Al 99.99%, Cu 99.99%, Fe 99.99%) by induction melting in an alumina crucible under a controlled pure helium atmosphere flow. A major difficulty for this alloy preparation is the existence of a peritectic transformation at high temperature. This induces a macrosegregation during the cooling process which leads eventually to large inhomogeneities of composition in the ingot. So, the entire ingots ($\approx$5 g) were remelted by induction heating in a silica tube and rapidly quenched by planar-flow casting on a rotating copper wheel, under a pure helium atmosphere. All of the samples studied were prepared with this method. The as-quenched state is two phased: the icosahedral phase, denoted as **I**, is accompanied by a small amount of a simple cubic FeAl-type phase, relegated to the interdendritic regions.

The as-quenched flakes were then annealed under ultrahigh vacuum in order to allow samples to reach equilibrium. DTA (differential thermal analysis) measurements were carried out using a SETARAM microdifferential thermal analyser. Flakes (20 mg) were put into alumina crucibles, and heated and cooled at 10 $^\circ$C min^{-1} under a pure argon flow.

Standard powder x-ray diffraction patterns were obtained on a Philips diffractometer equipped with a curved graphite monochromator in the diffracted beam, using Co Kα radiation ($\lambda = 1.7902$ Å). The instrument resolution, measured as the full width at half-maximum (FWHM) of the (200) line from a standard CeO_2 powder sample, was about $0.08^\circ\ \theta$ ($\Delta q \sim 1.5 \times 10^{-3}$ Å^{-1}), with $q = 2(\sin\theta)/\lambda$.

High-resolution x-ray diffraction experiments were performed using the synchrotron radiation on the line D-23 of LURE-DCI, equipped with a double-crystal monochromator (Si 111) in the incident beam and an analyser crystal (Ge 111) in the diffracted beam. At the wavelength chosen (1.7902 Å), the instrument resolution, measured as the FWHM of the (111) line of the standard Si powder sample, was about $0.01^\circ\ \theta$ ($\Delta q \sim 2 \times 10^{-4}$ Å^{-1})

The specimens for TEM were prepared by thinning the annealed ribbons in a Gatan Dual ion mill. They were then observed in a JEOL 2000FX microscope and a TOPCON 002B, and high-resolution images and some of the diffraction patterns were obtained.

2.2. Diffraction indexing

The indexing of the diffraction patterns of the icosahedral and approximant phases has been performed in the scheme proposed by Cahn *et al* [22] (for 3D periodic approximant phases, we also give the standard crystallographic indexing).

We use the 'shear' formalism as proposed several years ago by Jarić and Qiu [21], Janssen [23] and Yamamoto (see [24, 25]) for periodic approximants and recently extended to non-periodic approximants by Gratias *et al* [20].

The technique consists in developing a linear 'shear' field on the hyperlattice of the parent quasicrystal along the perpendicular space denoted as $\boldsymbol{E}_\perp$. The shear transformation is characterized by a 3×3 real matrix, say ε, defined as follows.

Consider a hyperlattice node with coordinates $\{\boldsymbol{x}_\parallel, \boldsymbol{x}_\perp\}$ in respectively the physical space denoted as $\boldsymbol{E}_\parallel$ and the perpendicular space, denoted as $\boldsymbol{E}_\perp$. The shear transformation sends this node to a new location $\{\boldsymbol{x}'_\parallel, \boldsymbol{x}'_\perp\}$:

$$\begin{cases} \boldsymbol{x}'_\parallel = \boldsymbol{x}_\parallel \\ \boldsymbol{x}'_\perp = \boldsymbol{x}_\perp - \boldsymbol{\varepsilon}\, \boldsymbol{x}_\parallel \end{cases} \tag{1}$$

which can be equivalently written in Fourier space as

$$\begin{cases} \boldsymbol{q}'_\parallel = \boldsymbol{q}_\parallel + {}^{\mathrm{t}}\boldsymbol{\varepsilon}\, \boldsymbol{q}_\perp \\ \boldsymbol{q}'_\perp = \boldsymbol{q}_\perp \end{cases} \tag{2}$$

where $\{\boldsymbol{q}_\parallel, \boldsymbol{q}_\perp\}$ are the coordinates of a wave vector of the initial reciprocal hyperlattice and $\{\boldsymbol{q}'_\parallel, \boldsymbol{q}'_\perp\}$ those of the transformed wave vector under the action of the shear.

Table 1. The number ν of split orbits and multiplicities μ for the principal reflections of the icosahedral symmetry as functions of the point symmetry of the approximant.

Icosahedral		Pentagonal		Cubic		Trigonal		Orthorhombic	
$m35$		$\bar{5}m$		$m3$		$\bar{3}m$		mmm	
Symmetry	μ	ν	μ	ν	μ	ν	μ	ν	μ
A_5	12	2	(2, 10)	1	12	2	(6, 6)	3	(4, 4, 4)
A_3	20	2	(10, 10)	2	(8, 12)	3	(2, 6, 12)	4	(4, 4, 4, 8)
A_2	30	3	(10, 10, 10)	2	(6, 24)	4	(6, 6, 6, 12)	6	(2, 2, 2, 8, 8, 8)

A symmetry breaking occurs when going from the (high-symmetry) parent quasicrystal to its approximants. This results in a splitting of the reflections characteristic of the point symmetry of the approximant. Table 1 shows the splitting scheme and the corresponding multiplicities of the most important reflections of the icosahedral phase for those symmetry subgroups that will be of interest in this paper. Similarly, table 2 shows the corresponding shear matrices. These matrices depend on one or several continuous parameter(s), depending of the symmetry stratum, which characterize(s) the shear amplitude in 6D space. The smaller these parameters are, the 'closer' to the icosahedral phase the approximant is.

Obviously, this shear technique is not meant to be representative of the actual physical process involved in the transformation where atomic diffusion seems to be a major factor in the transformation rate. It is used here as a convenient geometric tool for deciphering the strong similarities that exist between the unit cell of the approximant and a finite piece of the parent quasicrystal. Most of the atom sites in the approximant phase can be viewed as the results of a set of collective atom flips of the parent quasicrystal (some with an associated change in the chemical species), so large portions of medium-range-size atomic clusters are present in both structures. Loosely speaking, both structures are built essentially with roughly the same atomic units but stacked in a different way.

3. Description of the equilibrium phase diagram around 700 °C

3.1. The phase diagram

The isothermal section at 700 °C of the Al–Cu–Fe phase diagram near the icosahedral phase **I** is presented in figure 1.

At 700 °C three main single-phase domains are present corresponding to approximants. They are listed below.

Table 2. Shear matrices generating the approximants of the Al–Cu–Fe system. The symmetry-adapted bases are defined as follows: for the pentagonal and rhombohedral strata, the x-axis is along respectively the fivefold direction $(1, \tau, 0)$ and the threefold direction $(1, 1, 1)$, $\boldsymbol{y}$ is along a twofold direction perpendicular to $\boldsymbol{x}$, and $\boldsymbol{z}$ is a direction orthogonal to both. For the cubic and orthorhombic strata, the symmetry-adapted basis is identical to the standard basis.

Symmetry	ε on a symmetry-adapted basis	ε on the standard basis (three orthogonal twofold axes)
P		
(pentagonal: $\bar{5}m$)	$\tan\varphi \begin{pmatrix} 1 & 0 & 0 \\ 0 & 0 & 0 \\ 0 & 0 & 0 \end{pmatrix}$	$(\tan\varphi/\sqrt{5}) \begin{pmatrix} -1 & -\tau & 0 \\ \tau^{-1} & 1 & 0 \\ 0 & 0 & 0 \end{pmatrix}$
C		
(cubic: $m\bar{3}$)	$\tan\varphi \begin{pmatrix} 1 & 0 & 0 \\ 0 & 1 & 0 \\ 0 & 0 & 1 \end{pmatrix}$	$\tan\varphi \begin{pmatrix} 1 & 0 & 0 \\ 0 & 1 & 0 \\ 0 & 0 & 1 \end{pmatrix}$
O		
(orthorhombic: mmm)	$\begin{pmatrix} \tan\varphi & 0 & 0 \\ 0 & \tan\theta & 0 \\ 0 & 0 & \tan\gamma \end{pmatrix}$	$\begin{pmatrix} \tan\varphi & 0 & 0 \\ 0 & \tan\theta & 0 \\ 0 & 0 & \tan\gamma \end{pmatrix}$
R		
(trigonal: $\bar{3}m$)	$\begin{pmatrix} -\tan\varphi & 0 & 0 \\ 0 & \tan\theta & 0 \\ 0 & 0 & \tan\theta \end{pmatrix}$	$(1/6) \begin{pmatrix} a & b & c \\ c & a & b \\ b & c & a \end{pmatrix}$
		$\begin{cases} a = 2\tan\varphi + \tan\theta \\ b = 2\tan\varphi + (1 - 3\tau)\tan\theta \\ c = 2\tan\varphi + (3\tau - 2)\tan\theta \end{cases}$

(i) A *pentagonal* approximant **P1** with point group $\bar{5}m$, around the composition $Al_{63.6}Cu_{24.5}Fe_{11.9}$, first identified by Bancel [11]. This phase is a 1D periodic structure along the fivefold axis. The 1D lattice parameter is equal to 52.31 Å.

(ii) A *rhombohedral* approximant **R** with space group $R\bar{3}m$, extending from $Al_{63.4}Cu_{25}Fe_{11.6}$ to $Al_{61.6}Cu_{28}Fe_{10.4}$, first identified by Audier and Guyot [6] in a $Al_{63.5}Cu_{24}Fe_{12.5}$ sample. This phase is a 3D periodic structure, in which the unit cell is a rhombohedron with an angle equal to 36° and a lattice parameter equal to 32.14 Å.

(iii) An *orthorhombic* approximant **O** with space group *Immm*, around the composition $Al_{60.3}Cu_{30}Fe_{9.7}$. This phase is a 3D periodic structure with a unit cell with $a = 32.16$ Å, $b = 116.34$ Å, $c = 19.85$ Å.

The x-ray diffraction powder spectra are shown in figure 2 (see appendix A for a complete list of peak positions).

All of these approximants become icosahedral (imperfect) at high temperature; the transformation occurs between 715 °C and 740 °C, depending on the composition. They transform to the rhombohedral state below about 680 °C.

The transformations **I** $\rightleftharpoons$ approximants(**P1**, **R**, **O**) $\rightleftharpoons$ **R** are thermodynamically reversible. However, the kinetics is very sluggish when the initial state is not the as-quenched state (the defects introduced by the quench process increase the transformation rate).

The three domains of the approximants are located on a composition line parallel to the line of stability of the icosahedral phase. This agrees with the idea that these phases are stabilized by their electronic structure. With a given set of values for the number of valence

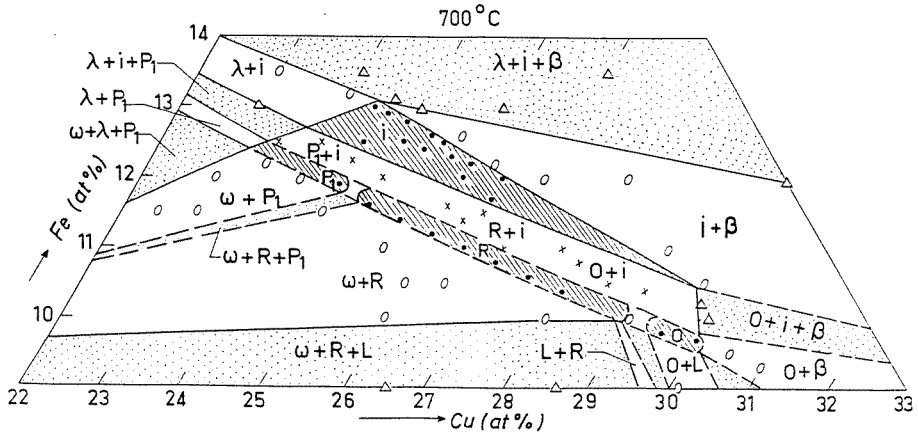

Figure 1. An isothermal section at 700 °C of the Al–Cu–Fe phase diagram showing the domains of the perfect icosahedral phase and its approximants: **P1** (pentagonal with a periodicity of 52.31 Å); **R** (rhombohedral); and **O** (orthorhombic) phases. The symbols have the following meanings: △: three-phase domain; *0*: two-phase domain; ● : one-phase domain; ×: at least two-phase domain, but the differences of the concentration and structure of the phases are so small that the determination of the tie-lines is not possible. Broken lines indicate an approximate boundary of a phase domain (a precise determination is impossible owing to the small difference of concentration). Inside the icosahedral domain there is a region around $Al_{62}Cu_{25.5}Fe_{12.5}$ where the perfect icosahedral phase remains unchanged on annealing at any lower temperature. The characteristics of such other crystalline phases as β, λ and ω can be found in [5, 26].

electrons of the three atomic species, the electronic concentrations of all of the alloys are distributed on parallel lines with a given slope, each line corresponding to a constant value of the electron/atom ratio (e/a). The slopes of the two experimental strips corresponding to single-phase alloys are compatible with reasonable values for the valencies of the atoms. Taking the values 3, 1 and -2 for respectively Al, Cu and Fe (for a detailed discussion of the negative valencies see [27]), we find that these lines would correspond to $e/a \sim 1.86$ for the icosahedral phase domain and $e/a \sim 1.92$ for the approximant domains.

Table 3 summarizes the results for the alloys studied along the two strips: it shows the composition of the alloys, the temperature of the solidus† determined by DTA measurements, the structural state at 700 °C and 730 °C, and the 6D lattice parameters. For the $Al_{63.4}Cu_{25}Fe_{11.6}$ alloy three phases (**R**, **P1**, **I**), which are well characterized, can be successively obtained after isothermal annealing at increasing temperature, from 680 °C to 740 °C (figure 3). The pentagonal phase **P1** is stable in a narrow domain of temperature around 710 °C: as is shown in the following scheme, **P1** can be obtained at 710 °C either from as-quenched icosahedral samples or from rhombohedral ones:

$$\begin{array}{lcl} \text{as-quenched}\ \mathbf{I} & \xrightarrow{\text{four days, 710 °C}} & \mathbf{P1} \\ & & \uparrow\ \text{four days, 710 °C} \\ \text{as-quenched}\ \mathbf{I} & \xrightarrow{\text{4 days 680 °C}} & \mathbf{R} \end{array}$$

† The knowledge of the solidus is obviously an important point since phases out of equilibrium can appear during cooling when a partial melting occurs during an isothermal annealing. This could lead to an erroneous interpretation of the phase diagram.

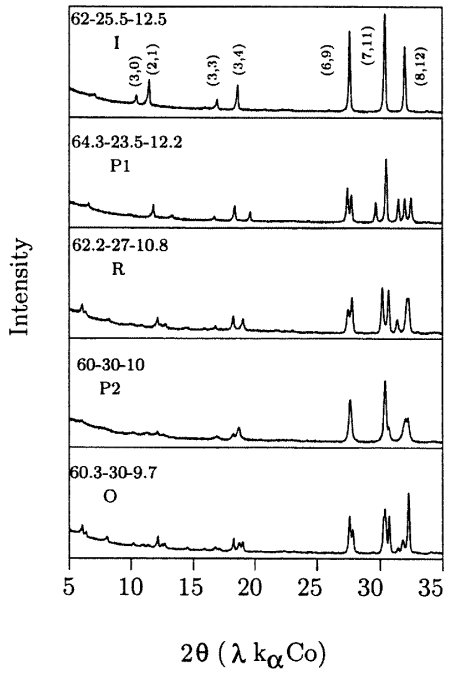

Figure 2. The x-ray powder diffraction pattern of the four approximants compared to the icosahedral one: **I** (the icosahedral phase); **P1** (the pentagonal approximant with 52.31 Å periodicity along the fivefold axis); **P2** (the pentagonal approximant with 84.49 Å periodicity along the fivefold axis); **O** (the orthorhombic approximant); and **R** (the rhombohedral approximant).

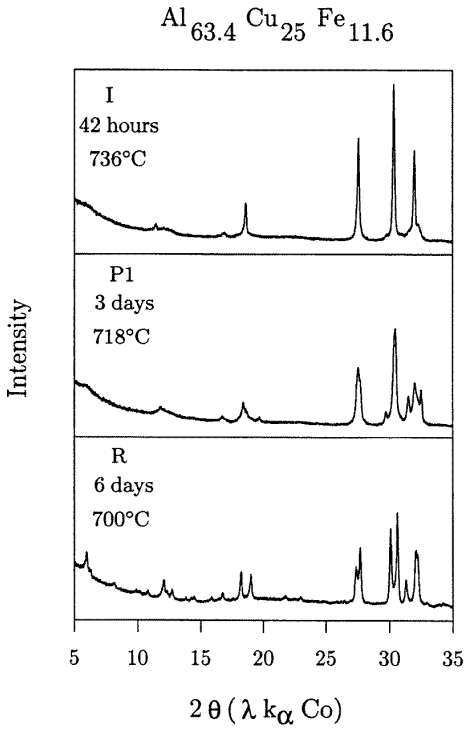

Figure 3. X-ray powder diffraction patterns of the $Al_{63.4}Cu_{25}Fe_{11.6}$ alloy for various values of the annealing temperature.

The morphology of the **P1** phase is shown in figure 4; numerous defects are present, but their nature is not elucidated yet. The grain size attained is several microns.

The rhombohedral approximant ($\alpha = 36^\circ$, 32.127 Å $< a <$ 32.160 Å depending on composition) corresponds to the structure first observed by Audier and Guyot [6, 7] for a $Al_{63.5}Cu_{24}Fe_{12.5}$ alloy. In Audier's paper the rhombohedral approximant is obtained below 650 °C as a 'microcrystalline phase' with a coherence length of some hundreds of Å. In contrast with this result, the single-phase rhombohedral samples obtained here have a grain size which can reach several microns (see, for example, the twins in the $Al_{63.8}Cu_{26}Fe_{11.2}$ alloy annealed for eleven days at 700 °C; figure 4). When we studied the composition chosen by Audier we found that, at 600 °C, whatever the annealing time, the x-ray diffraction peaks remain broad and the spectra are difficult to analyse; for us, that is an imperfect icosahedral state with large phason strains [28]. For this composition, we never obtained single-phase rhombohedral samples, probably due to the slow kinetics of the transformations.

At 700 °C the single-phase domain of the rhombohedral phase extends from $Al_{63.4}Cu_{25}Fe_{11.6}$ to $Al_{61.6}Cu_{28}Fe_{10.4}$. The transformation $\mathbf{I} \rightleftharpoons \mathbf{R}$ is reversible. The transformation $\mathbf{R} \rightarrow \mathbf{I}$ occurs rapidly at ≈735 °C, but the return to the **R** phase is slower: the reaction, performed at lower temperature (around 710 °C), is really slow and therefore

Table 3. Typical features of the various alloys studied with the following nomenclature for the quoted phases: **I**: icosahedral; **R**: rhombohedral; **P1**: pentagonal with 1D periodicity equal to 52.31 Å; **O**: orthorhombic (with 6D parameters A, B, C); **L**: liquid.

Al	Cu	Fe	T (°C) Solidus	The structural state after an annealing at 700 °C and the 6D lattice parameter in Å		The structural state after an annealing at 730 °C and the 6D lattice parameter in Å	
64.3	23.5	12.2	742	**P1** (+traces of ω)	6.3180	**P1** + **I** (no traces of ω)	6.3181
64.0	24.0	12.0	751	**P1** (+traces of ω)		**P1** + **I** (no traces of ω)	6.3167
63.6	24.5	11.9	748	**P1**		**P1** + **I**	6.3168
63.4	25.0	11.6	744	**R**	6.3109	**I**	6.3149
63.1	25.5	11.4	736	**R**	6.3109	**I**	6.3138
62.8	26.0	11.2	731	**R**	6.3091	**I**	6.3125
62.5	26.5	11.0	730	**R**	6.3067	**I**	6.3111
62.2	27.0	10.8	728	**R**	6.3068	**L** + **I**	6.3108
61.9	27.5	10.6	726	**R**	6.3058	**L** + **I**	6.3096
61.6	28.0	10.4	721	**R**	6.3044	**L** + **I**	6.3088
60.7	29.5	9.8	715	**O**		**L** + **I**	
60.3	30.0	9.7	711	**O**	$A = B =$ 6.3102 $C =$ 6.3029	**L** + **I**	
62.6	24.4	13.0	840	**I**	6.3198	**I**	6.3198
62.5	24.6	12.9	838	**I**	6.3193	**I**	6.3193
62.3	24.9	12.8	834	**I**	6.3180	**I**	6.3180
62.1	25.3	12.6	830	**I**	6.3173	**I**	6.3173
62.0	25.5	12.5	828	**I**	6.3176	**I**	6.3176

reaches completion with difficulty. A perfect single-phase rhombohedral structure is obtained only from an as-quenched icosahedral sample.

From the as-quenched icosahedral $Al_{60.3}Cu_{30}Fe_{9.7}$ alloy, four different phases (**R**, **O**, **P2**, **I**) can be obtained depending on the annealing temperature (figure 5). The rhombohedral phase **R** is stable up to 680 °C. The orthorhombic phase **O** seems to be stable in a narrow domain of temperature between 690 °C and 705 °C; the **O** phase can be obtained either from the rhombohedral state or the icosahedral one. Its morphology is shown in figure 4. The grain size (a few μm) is comparable to the size of the icosahedral grains. Extended defects of unknown nature cross the grains.

A pentagonal approximant **P2** with a lattice parameter along the fivefold axis equal to 84.49 Å was first identified by Menguy *et al* (see [12, 13]) by electron microscopy, in a $Al_{63.5}Cu_{24}Fe_{12.5}$ alloy. The composition that we find for **P2** is slightly different from the one given by Menguy *et al*: we find **P2** in the region of the orthorhombic phase **O** after the annealing at 708–710 °C of as-quenched samples. However, **P2** is never obtained in strictly single-phased form and cannot be obtained from the orthorhombic phase: annealing a single-phase **O** sample at 708–710 °C leads to a two-phase **O**+**I** state. Therefore, **P2** seems to be an intermediate metastable phase. In the electron micrograph in figure 4, the **P2** phase appears as small precipitates inside icosahedral grains. Such a result is in agreement with x-ray high-resolution experiments at LURE (see table A3).

Annealed at high temperature, all of the alloys studied transform into icosahedral phases. The corresponding 6D lattice parameters A are shown in figure 6. These parameters align

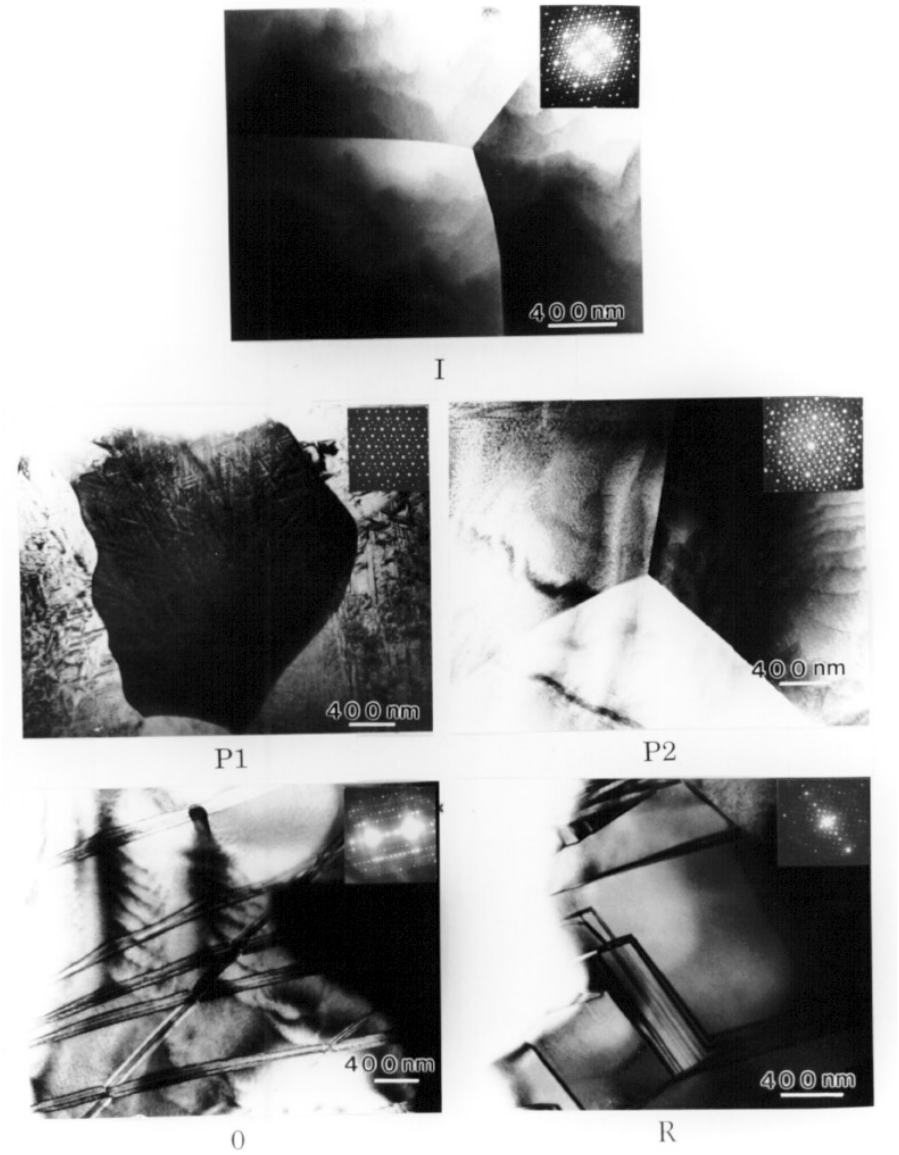

Figure 4. Electron micrographs showing the morphology of the different phases studied: **I** (the icosahedral phase, $Al_{62}Cu_{25.5}Fe_{12.5}$ alloy annealed for four hours at 795 °C); **P1** (the pentagonal approximant with 52.31 Å periodicity along the fivefold axis, $Al_{64}Cu_{24}Fe_{12}$ alloy annealed for four days at 710 °C); **P2** (the pentagonal approximant with 84.49 Å periodicity along the fivefold axis, $Al_{60.3}Cu_{30}Fe_{9.7}$ alloy annealed for six days at 708 °C); **O** (the orthorhombic approximant, $Al_{60.3}Cu_{30}Fe_{9.7}$ alloy annealed for eight days at 705 °C); and **R** (the rhombohedral approximant, $Al_{62.8}Cu_{26}Fe_{11.2}$ alloy annealed for eleven days at 700 °C).

along two parallel straight lines (with black and white dots) corresponding to the two values of the ratio e/a. Each group follows a typical law of ideal solid solution where the substitution for 1 Cu of 0.6 Al + 0.4 Fe increases the lattice parameter linearly (the value of the Goldschmidt atomic radius is 1.43 Å, 1.28 Å and 1.27 Å respectively for Al, Cu and

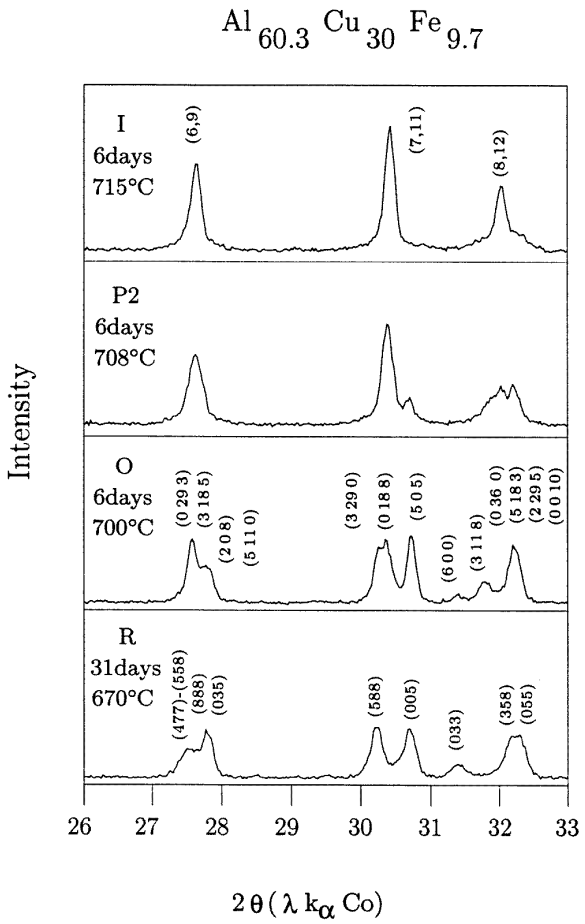

Figure 5. X-ray powder diffraction patterns of the $Al_{60.3}Cu_{30}Fe_{9.7}$ alloy for various values of the annealing temperature.

Fe). However, if we perform a comparison of the two groups we can see that:

(i) at constant concentration of Al, the lattice parameter decreases when Fe is substituted for with Cu;

(ii) at constant concentration of Cu, the lattice parameter decreases when Fe is substituted for with Al (whereas an increase of the parameter would be expected!)

It seems that a substitution involving only two kinds of atom is not possible, and perhaps the deviation from the stoichiometry is accomplished in reality by the creation of vacancies.

The variation of A calculated from the 3D lattice parameter of the periodic rhombohedral phase is also displayed in figure 6. The 6D cubic cell corresponding to the rhombohedral state is smaller than the 6D cubic cell of the high-temperature icosahedral state.

3.2. Crystallography of the approximant phases

The crystallographic characteristics in 6D space of the approximants of the icosahedral phase in the system Al–Cu–Fe are displayed in table 4. A convenient method for discussing the structure of these phases in 6D space consists in introducing one representative, say $\boldsymbol{E}_c$, of the 3D subspaces, whose images under the shear are 3D subspaces parallel to $\boldsymbol{E}_\parallel$; the

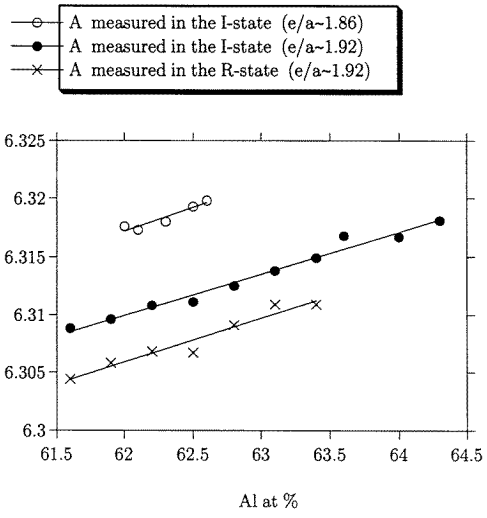

Figure 6. Variation of the 6D lattice parameter A as a function of the Al concentration.

Table 4. Approximant phases identified in Al–Cu–Fe. The different columns give: No 1: the symmetry of the approximant; No 2: the period in the 6D hyperspace; No 3: p/q (where $p, q \in \mathbb{Z}$), a ratio that characterizes the periodic approximant (see for instance figure 8 in which the node (r, s) has to be replaced by $(2p - q, q)$); No 4: the rational vectors of the 6D unit cell; No 5: the symmetry of these 6D vectors; No 6: the angles, present in the ε-matrix, that define the amplitude of the shear (see figure 8); No 7: the period of the approximants in the 3D physical space; No 8: the angles of the unit cell in the 3D physical space.

	6D					3D	
Symmetry	Period (in Å)	p/q	Unit cell	Symmetry	Angles of the ε-matrix	Period (in Å)	Angles
P1 [11]							
pentagonal	6.318	4/3	$5, 3, 3, 3, 3, \bar{3}$	5	$\varphi = -8.30°$	52.31	
($\bar{5}m$)							
R [6]			$3, 3, 2, 0, 2, 0$	2	$\varphi = 0.75°$		
rhombohedral	6.307	3/2	$3, 2, 3, 2, 0, 0$	2		32.14	36°
($R\bar{3}m$)			$2, 3, 3, 0, 0, 2$	2	$\theta = -5.15°$		
P2 [12, 13]							
pentagonal	6.307	7/4	$10, 4, 4, 4, 4, \bar{4}$	5	$\varphi = 3.19°$	84.49	
($\bar{5}m$)							
O	6.310	3/2	$0, 2, 3, 0, \bar{2}, 3$	2	$\varphi = -1.97°$	32.16	90°
orthorhombic	6.310	11/7	$11, 0, 7, 11, 0, \bar{7}$	2	$\theta = -0.75°$	116.34	90°
($Immm$)	6.303	2/1	$1, 2, 0, \bar{1}, 2, 0$	2	$\gamma = 5.15°$	19.85	90°

approximant structure can be seen as resulting from a cut of the atomic surfaces (properly reshaped for avoiding short distances) by $\boldsymbol{E}_c$, followed by a projection of the collected points into $\boldsymbol{E}_\parallel$. Hence, each approximant is characterized by a given $\boldsymbol{E}_c$ in the basic 6D space. A representation of the traces of the various $\boldsymbol{E}_c$-spaces corresponding to all four approximants is shown in figure 7 in the fivefold plane of the 6D space. Also shown in the figure are the traces of the atomic surfaces used to describe the icosahedral phase in Al–Cu–Fe as proposed by Katz and Gratias [29] where the icosahedral phase is represented by three atomic surfaces: a triacontahedron τ times larger than the standard one used to

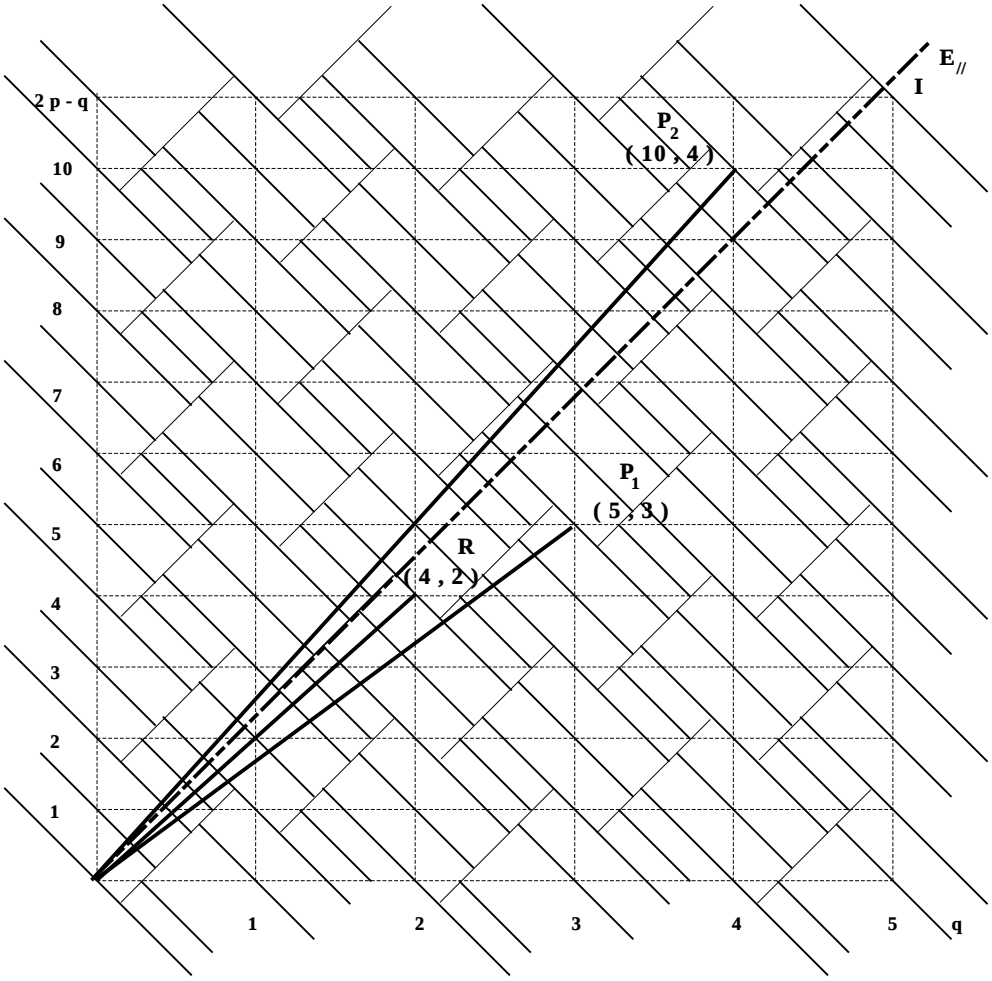

Figure 7. Traces of the cut spaces generating the approximants in Al–Cu–Fe in the fivefold plane in 6D (the trace of the cut space of the orthorhombic approximant **O** is the same as the one of **P2**). The characteristics of this representation are described in section 3.2.1.

generate the 3D Penrose tiling, centred at the site $n = \{0, 0, 0, 0, 0, 0\}$; the same object but truncated along the fivefold direction at the site $n' = \{1, 0, 0, 0, 0, 0\}$; and finally a triacontahedron τ times smaller than the standard one at the site $bc = \{1, 1, 1, 1, 1, 1\}/2$.

3.2.1. Pentagonal approximants. Pentagonal approximants are well known approximants of the Al–Cu–Fe system [11–14]. They are 1D periodic structures along the fivefold axis. As shown in table 2, the pentagonal stratum depends on one unique continuous parameter φ. This parameter corresponds to the tilt angle between the traces of $\boldsymbol{E}_{\parallel}$ and $\boldsymbol{E}_{\mathrm{c}}$ in the fivefold plane of the 6D space as shown in figure 8. A 1D periodic pentagonal phase is thus obtained by bringing in $\boldsymbol{E}_{\parallel}$ a node of type $\{r, s, s, s, s, \bar{s}\}$, with $r, s \in \mathbb{Z}$, while keeping invariant all lattice points in the other directions, so figure 8 is a faithful geometric representation of the shear mechanism.

It is straightforward to calculate the peak locations in the diffraction spectrum using

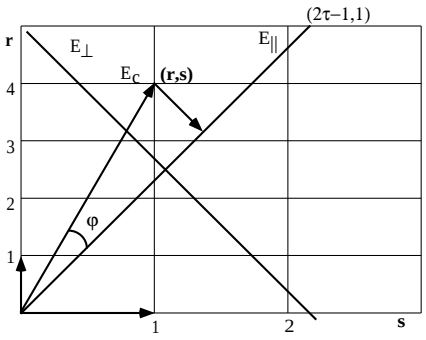

Figure 8. Pentagonal approximants can all be described by a shear of amplitude φ along the trace of the perpendicular space $\boldsymbol{E}_\perp$ in the fivefold plane of the parent icosahedral structure. After the shear, the node (r, s) aligns along the physical space $\boldsymbol{E}_\parallel$ (the coordinates of any point that belongs to a fivefold plane are $\{x, y, y, y, y, -y\}$ which are replaced in the figure by the notation (x, y)).

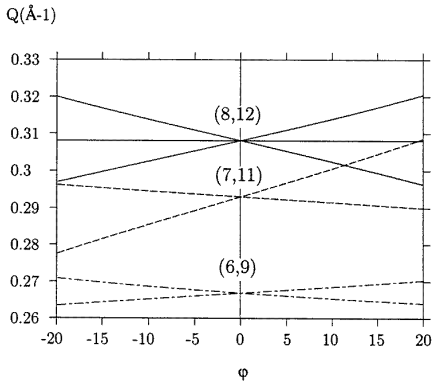

Figure 9. Splitting, as a function of the angle φ, of the typical triplet of reflections (6, 9), (7, 11), (8, 12).

equations (2) and the expression for the corresponding $\varepsilon(\varphi)$-matrix (see table 2); the lengths of the diffraction wave vectors, denoted as $\boldsymbol{Q}$, in the pentagonal approximants are related to those of the icosahedral phase, denoted as $\boldsymbol{q}$, by

$$Q^2 = q^2 + 2q_{\parallel,5}q_{\perp,5}\tan\varphi + q_{\perp,5}^2\tan^2\varphi \tag{3}$$

where $q_{\parallel,5}$ and $q_{\perp,5}$ are the components of the icosahedral wave vector along the pentagonal direction in respectively $\boldsymbol{E}_\parallel$ and $\boldsymbol{E}_\perp$:

$$q_{\parallel,5} = \boldsymbol{q}\cdot\boldsymbol{e}_x^\parallel \qquad q_{\perp,5} = \boldsymbol{q}\cdot\boldsymbol{e}_x^\perp \qquad q^2 = \frac{N + M\tau}{2(2+\tau)}. \tag{4}$$

The vectors $\boldsymbol{e}_x^\parallel$ and $\boldsymbol{e}_x^\perp$ are the unit vectors along fivefold directions in respectively $\boldsymbol{E}_\parallel$ and $\boldsymbol{E}_\perp$:

$$\begin{cases} \boldsymbol{e}_x^\parallel = (1/\sqrt{10})\{\sqrt{5}, 1, 1, 1, 1, -1\} \\ \boldsymbol{e}_x^\perp = (1/\sqrt{10})\{\sqrt{5}, -1, -1, -1, -1, 1\}. \end{cases} \tag{5}$$

The peak locations of the typical triplet of reflections of the icosahedral phase (6, 9), (7, 11) and (8, 12) versus φ are shown in figure 9. This figure can be used as an 'abacus' for a direct reading of the φ-angle from the experimental position of these three groups of reflections: the angle φ is obtained by matching the experimental peak locations with the corresponding abacus's lines.

We obtain the following values of the angle.

(i) For the pentagonal phase **P1**:

$\varphi = -8.30^\circ$ with a 6D lattice parameter $A = 6.3180$ Å.

(ii) For the pentagonal phase **P2**:

$\varphi = 3.19^\circ$with a 6D lattice parameter $A = 6.3070$ Å.

Tables A2 and A3 in the appendix can be consulted to appreciate the agreement between the calculated and observed peak positions.

Both values of φ correspond to $\boldsymbol{E}_c$-spaces that are 1D rational with respect to the 6D lattice. As the trace of $\boldsymbol{E}_\parallel$ in the fivefold plane is a line of slope $\pi/4$, it is easily shown that an $\boldsymbol{E}_c$-space containing the direction $\{r, s, s, s, s, \bar{s}\}$ makes with $\boldsymbol{E}_\parallel$ the angle φ, where

$$\tan\varphi = \frac{r - s\sqrt{5}}{r + s\sqrt{5}}. \tag{6}$$

The period along the fivefold axis is given by the projection onto $\boldsymbol{E}_\parallel$ of the node $\{r, s, s, s, s, \bar{s}\}$:

$$a = \frac{r - s + 2s\tau}{\sqrt{2}} A \tag{7}$$

where A denotes the 6D lattice parameter of the icosahedral phase.

An equivalent method, closer to the notion of rational approximants of the golden mean, consists in approximating the direction $\{2\tau - 1, 1, 1, 1, 1, -1\}$ which is the trace of $\boldsymbol{E}_\parallel$ in the fivefold plane (as $\sqrt{5} = 2\tau - 1$), by replacing the golden mean τ by one of its rational approximants p/q. We obtain the direction $\{2p-q, q, q, q, q, -q\}$ in 6D and the expression for the angle φ becomes

$$\tan\varphi = \frac{p - q\tau}{p - q + q\tau} \tag{8}$$

and the period a along the fivefold axis in $\boldsymbol{E}_\parallel$ becomes

$$a = \sqrt{2}A(p - q + q\tau) \tag{9}$$

(an expression similar to that of the rhombohedral parameter along a fivefold axis expressed in [8]). These two integers p and q are used for characterizing the two pentagonal phases **P1** and **P2**:

(i) for **P1** with $\varphi = -8.30^\circ$, we obtain $p = 4$, $q = 3$; the 1D lattice parameter is given by the projection of the node $\{5, 3, 3, 3, 3, \bar{3}\}$ onto $\boldsymbol{E}_\parallel$ leading to 52.31 Å;

(ii) for **P2** with $\varphi = 3.19^\circ$, we obtain $p = 7$ and $q = 4$; the 1D lattice parameter is given by the projection of the node $\{10, 4, 4, 4, 4, \bar{4}\}$ onto $\boldsymbol{E}_\parallel$ leading to 84.49 Å.

The identification of the pentagonal phases is confirmed by a study performed on TEM diffraction patterns as shown in figure 10 where experimental and computed diffraction patterns are compared. Simulations are performed with the algorithms described in section 2.2. The intensities of the reflections are represented by discs of radius $\propto \exp -|\boldsymbol{q}_\perp|$, where $\boldsymbol{q}_\perp$ is the (shortest) perpendicular component of the wave vector. This factor has been introduced to qualitatively mimic, as a guide to the eye, the usual intensity decay with increasing $|\boldsymbol{q}_\perp|$. Obviously, real approximants may show quite different intensity behaviour, especially for the reflections with large $|\boldsymbol{q}_\perp|$-values.

A detailed discussion about the 'systematic' extinctions exhibited along the fivefold direction in both pentagonal phases will be presented in a forthcoming paper.

3.2.2. Rhombohedral approximants. The rhombohedral approximant is the best known approximant of the Al–Cu–Fe system [6–10]. It is a 3D periodic phase belonging to the trigonal stratum with a rhombohedral lattice. The corresponding shear matrix (see table 2) has two parameters φ and θ which are experimentally found to be

$$\varphi = 0.75^\circ \qquad \theta = -5.15^\circ.$$

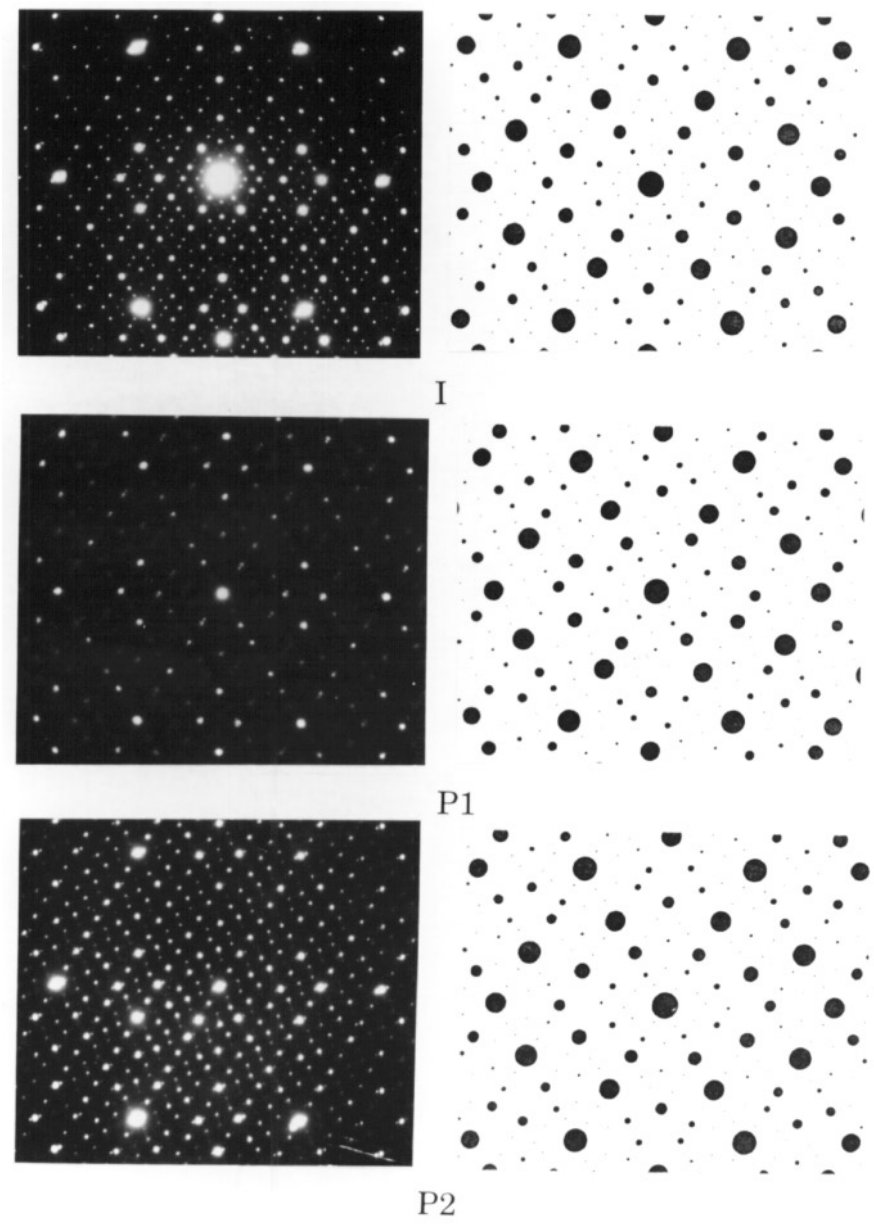

Figure 10. TEM diffraction patterns in twofold orientation and corresponding simulations performed for the icosahedral phase **I** and the two pentagonal phases **P1** and **P2**.

These two values can be obtained from one single pair of integers p and q (see table 4) via the relations

$$\tan\varphi = \frac{-(2p+q)+(p+q)\tau}{q+p\tau} \qquad \tan\theta = \frac{(p-q)+(p-2q)\tau}{q+p\tau}. \tag{10}$$

The 3D lattice parameters a and c in $\boldsymbol{E}_\parallel$ along respectively a twofold axis (a rhombohedral setting) and a threefold axis (a hexagonal setting) can be expressed as

$$a = \frac{\sqrt{2}A(q + p\tau)}{\sqrt{2+\tau}} \qquad c = \frac{\sqrt{6}A\,(p + (p+q)\tau)}{\sqrt{2+\tau}} \tag{11}$$

where A is the 6D lattice parameter.

The crystallographic characteristics of the periodic rhombohedral approximant are displayed in table 4. The unit vectors in 6D are of the type $\{p, p, q, 0, q, 0\}$ with $p = 3$ and $q = 2$ [8]. The angle between the trace of $\boldsymbol{E}_\mathrm{c}$ and the trace of $\boldsymbol{E}_\parallel$ in the corresponding twofold planes is -1.97° which shows that the shear amplitude is remarkably small. Table A1 in the appendix can be consulted to appreciate the agreement between the calculated and observed peak positions.

We observe that this rhombohedral approximant is characterized by a unique doublet of integers p and q, whereas the corresponding trigonal stratum has dimension 2. Indeed, since the shear field of the transformation corresponds in $\boldsymbol{E}_\perp$ to an extension/contraction along a threefold axis (characterized by the angle φ), and an independent extension/contraction developing axially in the perpendicular plane (characterized by the angle θ), we would expect two 'independent' doublets—say (p_φ, q_φ) and (p_θ, q_θ). This is indeed the case for trigonal approximants with a hexagonal lattice which are defined by two independent lattice parameters a and c. But it is not the case for rhombohedral lattices which are defined by one unique lattice parameter a having well defined components in both deformation subspaces: this imposes a relationship between the angles φ and θ and therefore reduces by one the number of independent doublets of integers needed to characterize the phase.

As for the pentagonal case, it is straightforward, although more complicated, to calculate the powder diffraction spectrum:

$$\begin{aligned} Q^2 = q^2 + 2\left(-q_{\parallel,3}q_{\perp,3}\tan\varphi + (q_{\parallel,2}q_{\perp,2} + q_{\parallel,m}q_{\perp,m})\tan\theta\right) \\ + q_{\perp,3}^2\tan^2\varphi + (q_{\perp,2}^2 + q_{\perp,m}^2)\tan^2\theta \end{aligned} \tag{12}$$

where $q_{\parallel,3}$, $q_{\parallel,2}$, $q_{\parallel,m}$ and $q_{\perp,3}$, $q_{\perp,2}$, $q_{\perp,m}$ are the components, in $\boldsymbol{E}_\parallel$ and $\boldsymbol{E}_\perp$, of the icosahedral wave vector along the three orthogonal directions, respectively: a threefold one of type (1,1,1), a twofold one and a direction belonging to a mirror. It can be noted that the expressions for the $\boldsymbol{e}_j^i$ present in the equation

$$q_{i,j} = \boldsymbol{q}\cdot\boldsymbol{e}_j^i \qquad \text{with } i = \parallel, \perp \text{ and } j = 3, 2, m$$

are given in [20].

The TEM diffraction patterns obtained for the rhombohedral phase and corresponding to the icosahedral twofold planes are compared, in figure 11, to the simulations (the calculation is similar to the one used in the pentagonal case).

3.2.3. Orthorhombic approximants. This phase, denoted as **O**, is a three-dimensional periodic phase with an orthorhombic symmetry of space group *Immm*. It has been identified by x-ray powder diffraction (see figure 2). The accurate determination of the splitting of the icosahedral reflections has been made using high-resolution diffraction (line D-23 at LURE-DCI) as shown in figure 12. The crystallographic parameters of this phase are given in table 4. This phase **O** has such large unit-cell parameters (in particular along one direction) that the use of a high-resolution x-ray diffractometer is necessary to separate the various peaks. As shown in figure 12, we can clearly see that the original (6, 9) icosahedral peak splits into four distinct peaks; each of them has a width close to the instrumental one, and

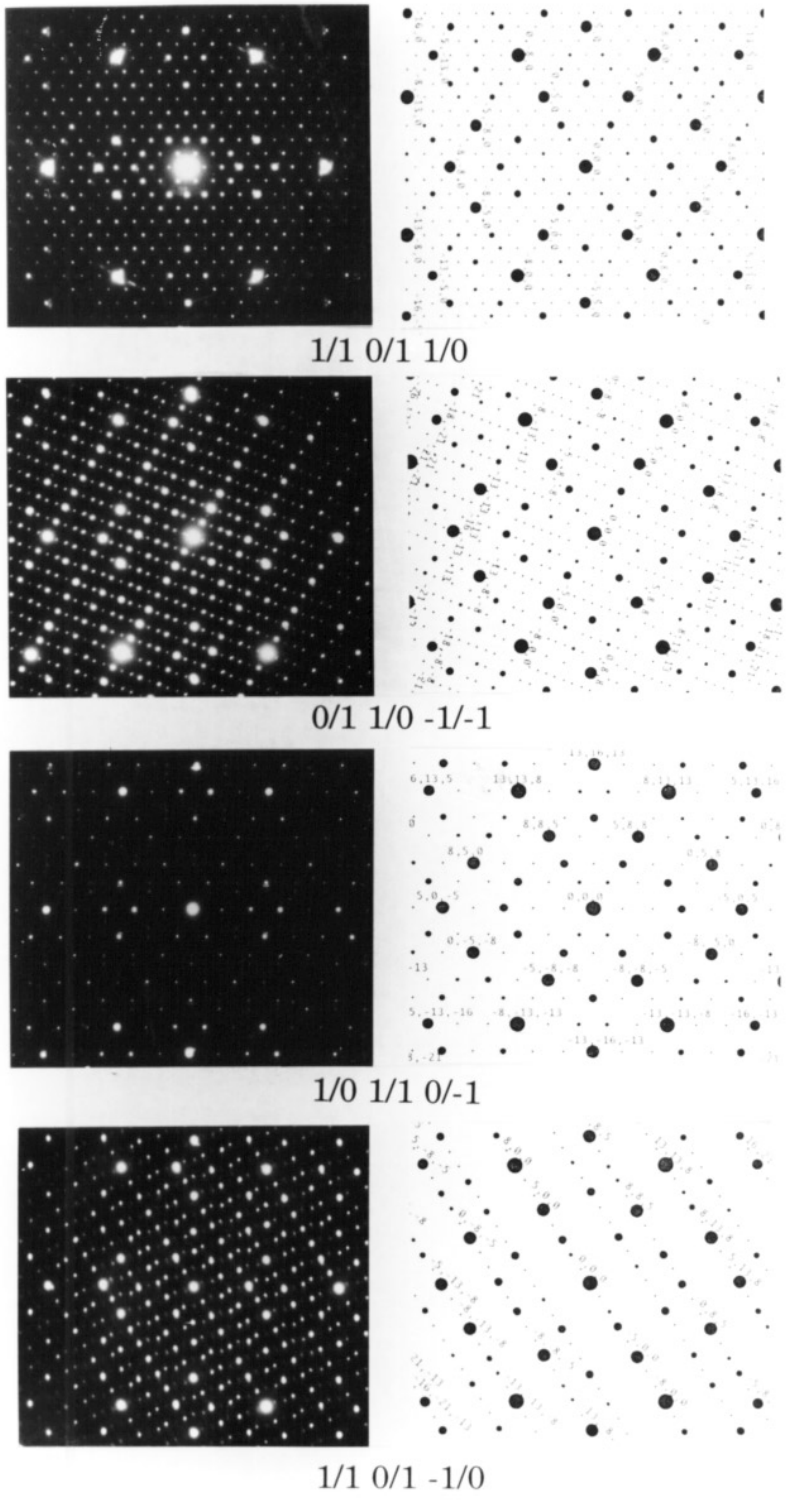

Figure 11. TEM diffraction patterns of the rhombohedral phase **R** in twofold orientation and corresponding simulations.

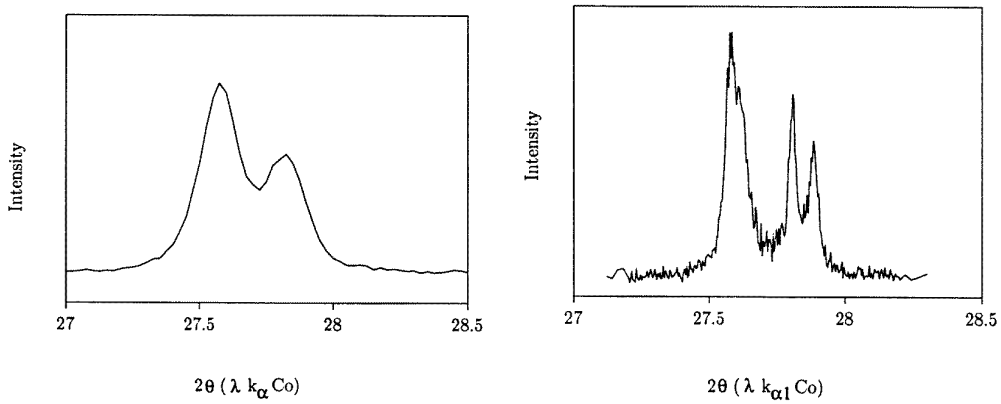

Figure 12. The orthorhombic phase **O**; the splitting of the x-ray reflection indexed as (6, 9) in the icosahedral scheme: (a) a scan on a standard diffractometer; (b) a scan on a high-resolution diffractometer (synchrotron radiation at LURE).

among these four peaks, two are especially close. Even with such a resolution, it has not been possible to fully separate all reflections.

Instead of building the general projector matrix corresponding to the orthorhombic stratum, we have calculated the shear matrix $\varepsilon_{mmm}(\varphi, \theta, \gamma)$ (expressed in table 2) directly from the shear matrix of the cubic stratum $\varepsilon_{m\bar{3}}(\varphi)$ (table 2) in which the three orthogonal binary axes are considered as independent axes.

As the orthorhombic stratum has dimension 3, the shear field of the transformation corresponds in $\boldsymbol{E}_\perp$ to three independent deformation fields along the three twofold axes (characterized respectively by the angles φ, θ and γ). Periodic orthorhombic approximants are then characterized by three independent doublets of integers (p_φ, q_φ), (p_θ, q_θ) and (p_γ, q_γ).

The values of the angles that are in best agreement with the experimental x-ray diffracted data (table A4) are the following:

$$\varphi = -1.97^\circ \qquad \theta = -0.75^\circ \qquad \gamma = 5.15^\circ.$$

These values are related to the doublet of integers (p_α, q_α) by

$$\tan\alpha = \frac{p_\alpha - q_\alpha \tau}{q_\alpha + p_\alpha \tau} \tag{13}$$

where α stands for φ, θ and γ. The values of (p_α, q_α) are (table 4)

$$p_\varphi/q_\varphi = 3/2 \qquad p_\theta/q_\theta = 11/7 \qquad p_\gamma/q_\gamma = 2/1.$$

The corresponding 3D periodic orthorhombic structure has lattice parameters

$$a = 32.16 \text{ Å} \qquad b = 116.34 \text{ Å} \qquad c = 19.85 \text{ Å}.$$

The rhombohedral phase **R** and the orthorhombic phase **O** share the same value of p/q, namely $3/2$, and therefore the same 6D node, which gives a similar value of the 3D lattice parameter along this direction.

From the expression for the 3D lattice parameter along a twofold axis (a in equation (11)), the 6D parameters can be obtained from the three independent doublets (p_α, q_α):

$$A = 6.310 \text{ Å} \qquad B = 6.310 \text{ Å} \qquad C = 6.303 \text{ Å}$$

and we can notice that $A = B \neq C$. The 6D lattice of the orthorhombic phase **O** is no longer a (hyper)cubic lattice, as it is for the other periodic approximants, but is now a pseudo-cubic lattice with a tiny deformation of

$$\frac{\Delta A}{A} = \frac{A - C}{A} = 0.11\%.$$

As previously, the powder diffraction spectrum can be calculated as†

$$Q^2 = q^2 + 2\left(q_{\parallel,2_x} q_{\perp,2_x} \tan\varphi + q_{\parallel,2_y} q_{\perp,2_y} \tan\theta + q_{\parallel,2_z} q_{\perp,2_z} \tan\gamma\right) + q_{\perp,2_x}^2 \tan^2\varphi + q_{\perp,2_y}^2 \tan^2\theta + q_{\perp,2_z}^2 \tan^2\gamma \quad (14)$$

where $q_{\parallel,2_x}$, $q_{\parallel,2_y}$, $q_{\parallel,2_z}$ and $q_{\perp,2_x}$, $q_{\perp,2_y}$, $q_{\perp,2_z}$ are the components of the icosahedral wave vector along the three orthogonal twofold axes in, respectively, the parallel and perpendicular spaces. The locations of the principal peaks calculated with these values are displayed in table A4. The column headed $\delta q_{(\mathrm{theo-exp})}$ shows that the differences between experimental and theoretical values are within the accuracy of the experimental determination, i.e. 10^{-4}.

TEM diffraction patterns with the associated simulations (similar computations to those in the pentagonal and rhombohedral cases) are presented in figure 13 for several basic crystallographic planes. The two patterns perpendicular to the twofold axes $[0/2,\ 0/0,\ 0/0]$ and $[0/0,\ 0/2,\ 0/0]$ show the three basic periods; the first one reveals, in reciprocal space, the large period equal to 116.35 Å in the real space.

4. Conclusion

The present diffraction study shows a very good agreement between the experimental data and the theoretical predictions based on both simple symmetry considerations for inferring the possible splits of the icosahedral reflections and the shear formalism of the 6D lattice in perpendicular space for quantitative crystallographic information. Although this study is based only on the locations of the diffraction peaks and not on their relative intensities (no displacement field in parallel space has been introduced in the theoretical description), the results strongly support the idea that approximant structures have essentially the same kind of local order as their parent quasicrystalline phase with similar atomic units up to relatively large distances (several nanometres).

The extensive study of the equilibrium phase diagram of Al–Cu–Fe in the vicinity of the icosahedral phase shows that the icosahedral phase and its rhombohedral approximant *may* exist as fundamental states at 0 K in narrow domains of composition extending along two parallel lines in the phase diagram. These lines correspond to constant average outer-electron concentrations and their slope is compatible with reasonable values for the valencies of the atoms. Hence it may be thought that the electron structure plays a major role in the stabilization of the icosahedral and rhombohedral phases at low temperature. These lines of highest stability correspond also to a given law of substitution for Cu with Al and Fe, which allows the composition variation within the stability range. Outside the range of highest stability of the **I** phase, lattice parameter measurements show that the introduction of vacant sites is probably necessary to accommodate the composition; this behaviour would keep the electron concentration in the quasicrystal constant.

At increasing temperature the domain of the rhombohedral phase remains very narrow and even its extension decreases when the transformations to the pentagonal **P1** and orthorhombic phases occur. On the other hand, the domain of the **I** phase widens out as the temperature increases, becomes a maximum near 740 °C, and then decreases.

† This expression can be used if the 6D lattice is a strictly cubic lattice.

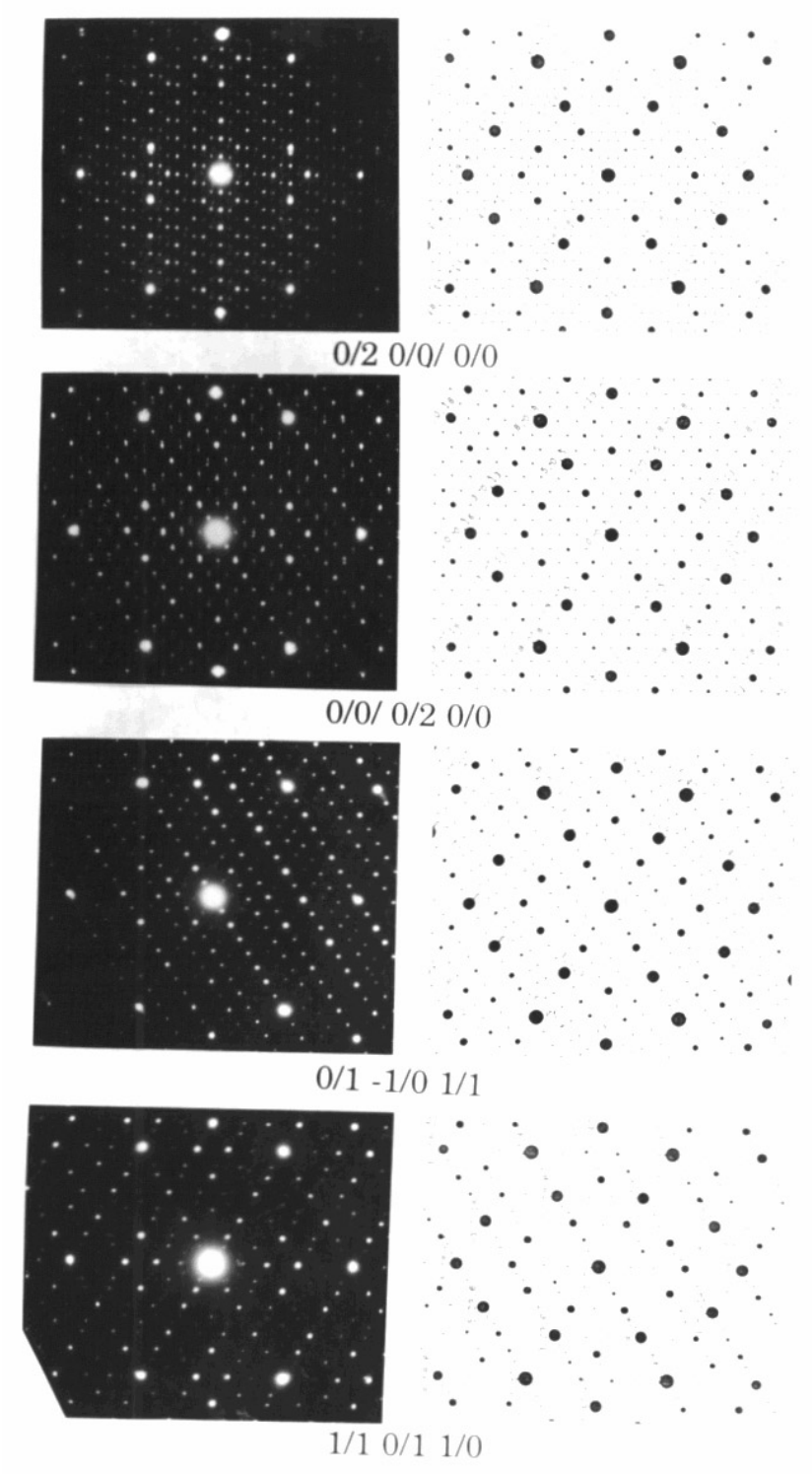

Figure 13. TEM diffraction patterns of the orthorhombic phase **O** in twofold orientation and corresponding simulations.

The reversible phase transformation between icosahedral and rhombohedral structures can be studied, without crossing the **P1** or the **O** domain, in alloys on the line of the phase diagram extending from $Al_{62.8}Cu_{26}Fe_{11.2}$ to $Al_{61.9}Cu_{27.5}Fe_{10.6}$. For all of these alloys a two-phase (**R** + **I**) domain exists at high temperature, above the rhombohedral domain; in a temperature range of 15 °C, different proportions of rhombohedral to icosahedral phase can be reversibly obtained. Above this two-phase domain the tip of the single-phase domain of the **I** phase (at ∼740 °C) may be crossed only for extremely controlled conditions of composition and temperature. More often, (**I** + liquid) or (λ-phase + **I** + liquid) mixtures are obtained. These observations suggest that the rhombohedral phase may not occur as a polymorphous transformation of the **I** phase, but rather as a (peritectic?) transformation from (**I** + λ + liquid). Experiments are in progress in order to obtain vertical sections of the phase diagram for constant Cu contents (25 and 26 at.%).

Several papers have been devoted to the icosahedral–rhombohedral transformation of the $Al_{63.5}Cu_{24}Fe_{12.5}$ alloy (see, for example, [13, 14] and references therein). They all conclude that the rhombohedral structure is stable at low temperature. According to [13, 14], a phase transition towards an icosahedral phase occurs at ∼675 °C via a transient state identified as the pentagonal phase **P2**, whereas the reverse transformation (icosahedral to rhombohedral) involves several transient states: first a modulated state of the **I** phase, then a mixing of the two pentagonal structures **P1** and **P2**. We never observed such a transformation at this same composition whatever the temperature. According to the present work, **P1** exists as a stable single phase in a narrow domain of composition and temperature (figure 1) and **P2** is found only as a transient state in the orthorhombic–icosahedral transformation of the $Al_{60.3}Cu_{30}Fe_{9.7}$ alloy.

The main purpose of the present work was the determination of the *equilibrium* phase diagram of Al–Cu–Fe and no attempt has been made to elucidate the mechanism of the phase transformations especially through possible transient states. This may explain the small differences found (concerning both the localization of the pentagonal phases in the phase diagram and the **I** ⇌ **R** transformation) between the results of [13, 14] and the present paper.

Acknowledgments

We are very grateful to Dr D Gratias for his critical and patient review of the manuscript. We are very pleased to thank Drs F Hippert, R A Brand and C Berger for fruitful discussions about the transport properties of the approximant phases described in this paper.

Appendix A

In the tables presented in this appendix: $\boldsymbol{q}$ represents the parallel component of the 6D diffraction vector, theoretical (theo) and experimental (exp) values are displayed with the difference of these values (theo − exp). The experimental values have been determined by a profile fitting. In the high-resolution experiments the order of magnitude of the error in the determination of the peak positions is $\Delta q = \pm 2 \times 10^{-5}$ Å^{-1}; with current experimental conditions this value is lowered to $\pm 2 \times 10^{-4}$ Å^{-1}. The full widths at half-maximum of the diffraction peaks of the best observed approximants are within the instrumental resolution in both standard and high-resolution experiments.

Table A1. Theoretical and experimental positions of the main reflections for the rhombohedral approximant **R** ($p/q = 3/2$) with 3D lattice parameter $a = 32.1394$ Å, tilt angles $\varphi = 0.75^\circ$ and $\theta = -5.15^\circ$. This phase of composition $Al_{62.2}Cu_{27}Fe_{10.8}$ is obtained after annealing for three days at 705 °C. The phase is icosahedral at 750 °C with the 6D primitive lattice parameter $A = 6.3068$ Å.

N	M	q_{ico} (Å^{-1})	h	k	l	μ	I	d_{theo} (Å)	q_{theo} (Å^{-1})	q_{exp} (Å^{-1})	$\delta q_{(theo-exp)}$ (10^{-4} Å^{-1})
6	$\bar{3}$	0.063 10	1	1	0	12	1	16.070	0.062 23	0.062 26	−0.298
6	$\bar{3}$	0.063 10	2	2	2	2		15.012	0.066 61		
6	$\bar{3}$	0.063 10	2	1	1	6		13.670	0.073 15		
3	$\bar{1}$	0.069 29	1	0	0	6	2	16.897	0.059 18	0.059 24	−0.582
3	$\bar{1}$	0.069 29	2	2	1	6	1	12.441	0.080 38	0.080 32	0.562
2	1	0.112 12	3	3	2	6	1	9.421	0.106 15	0.106 16	−0.125
2	1	0.112 12	2	0	0	6	2	8.448	0.118 37	0.118 27	0.959
3	4	0.181 41	3	0	0	6	4	5.632	0.177 55	0.177 53	0.243
3	4	0.181 41	5	5	3	6	3	5.396	0.185 33	0.185 01	3.203
6	9	0.267 29	8	5	5	6	6	3.770	0.265 24	0.265 11	1.266
6	9	0.267 29	8	8	8	2	6	3.753	0.266 46	0.266 06	3.921
6	9	0.267 29	5	3	0	12	10	3.724	0.268 51	0.268 38	1.247
7	11	0.293 53	8	8	5	6	14	3.435	0.291 16	0.290 95	2.058
7	11	0.293 53	5	0	$\bar{0}$	6	14	3.379	0.295 92	0.295 77	1.453
8	12	0.307 88	3	0	$\bar{3}$	6	5	3.311	0.302 07	0.302 02	0.420
8	12	0.307 88	8	5	3	12	9	3.231	0.309 46	0.309 21	2.421
8	12	0.307 88	5	5	0	6	9	3.214	0.311 14	0.310 85	2.960
8	12	0.307 88	10	8	8	6		3.213	0.311 19		
18	29	0.474 94	8	0	0	6	52	2.112	0.473 46	0.473 55	−0.875
18	29	0.474 94	13	13	8	6	72	2.099	0.476 42	0.476 19	2.291
20	32	0.499 38	8	8	0	6	100	2.009	0.497 83	0.497 51	3.195
20	32	0.499 38	16	13	13	6	75	2.009	0.497 84	0.497 76	0.818
20	32	0.499 38	13	8	$\bar{5}$	12	75	2.004	0.498 91	0.498 75	1.593
20	32	0.499 38	5	0	$\bar{5}$	6	23	1.986	0.503 44	0.503 27	1.697
52	84	0.808 02	8	0	$\bar{8}$	6	7	1.241	0.805 51	0.805 35	1.622
52	84	0.808 02	21	13	8	12	27	1.237	0.808 32	0.808 02	3.004
52	84	0.808 02	13	13	0	6	25	1.236	0.808 98	0.808 80	1.767
52	84	0.808 02	26	21	$\bar{21}$	6		1.236	0.808 98		
70	113	0.937 29	8	8	$\bar{8}$	6	3	1.070	0.934 35	0.934 58	−2.270
70	113	0.937 29	21	8	5	12	7	1.069	0.935 85	0.935 89	−0.437
70	113	0.937 29	29	26	21	12	4	1.067	0.936 78	0.937 56	−7.817
70	113	0.937 29	21	21	8	6		1.066	0.937 69		
70	113	0.937 29	26	$\bar{21}$	13	12		1.066	0.937 91		
70	113	0.937 29	13	$\bar{5}$	0	12	3	1.064	0.939 76	0.939 14	6.178
72	116	0.949 88	16	0	0	6	6	1.056	0.946 93	0.946 93	0.000
72	116	0.949 88	21	16	5	12		1.056	0.946 93		
72	116	0.949 88	29	21	18	12	5	1.055	0.947 50	0.947 60	−0.988
72	116	0.949 88	29	29	26	6	5	1.054	0.948 76	0.949 04	−2.792
72	116	0.949 88	26	13	$\bar{13}$	6		1.051	0.951 00		
72	116	0.949 88	13	8	$\bar{5}$	12	5	1.050	0.952 27	0.952 38	−1.089
72	116	0.949 88	18	8	0	12	3	1.049	0.952 83	0.953 11	−2.724
72	116	0.949 88	26	26	16	6		1.049	0.952 83		

Table A2. Theoretical and experimental positions of the main reflections for the pentagonal approximant **P1** ($p/q = 4/3$) with the 1D lattice parameter $a = 52.3064$ Å, and tilt angle $\varphi = -8.30°$. This phase of composition $Al_{64.3}Cu_{23.5}Fe_{12.2}$ is obtained after annealing for three days at 720 °C. The phase is icosahedral at 740 °C with the 6D primitive lattice parameter $A = 6.3180$ Å. Rows given in bold type show reflections that belong to the periodic fivefold axis.

N	M	q_{ico} (Å^{-1})	μ	I	d_{theo} (Å)	q_{theo} (Å^{-1})	q_{exp} (Å^{-1})	$\delta q_{(theo-exp)}$ (10^{-4} Å^{-1})
3	$\bar{1}$	0.069 17	10	1	15.444	0.064 75	0.064 31	4.44
3	**$\bar{1}$**	**0.069 17**	**2**	**1**	**10.461**	**0.095 59**	**0.095 66**	**−0.74**
2	**1**	**0.111 92**	**2**	**1**	**10.461**	**0.095 59**	**0.095 66**	**−0.74**
2	1	0.111 92	10	4	8.668	0.115 37	0.115 09	2.82
3	4	0.181 09	10	5	5.583	0.179 12	0.178 55	5.71
3	**4**	**0.181 09**	**2**	**3**	**5.231**	**0.191 18**	**0.190 63**	**−2.15**
6	9	0.266 81	10	12	3.767	0.265 44	0.264 94	4.97
6	9	0.266 81	10	10	3.727	0.268 28	0.267 81	4.71
7	**11**	**0.293 01**	**2**	**7**	**3.487**	**0.286 77**	**0.286 20**	**5.73**
7	11	0.293 01	10	22	3.398	0.294 27	0.293 82	4.46
8	12	0.308 09	10	8	3.295	0.303 44	0.302 99	4.46
8	12	0.308 09	10	8	3.246	0.308 09	0.307 78	3.12
8	12	0.308 09	10	9	3.196	0.312 85	0.312 30	5.45
12	16	0.362 18	10	1	2.889	0.346 13	0.345 52	6.11
12	16	0.362 18	10	2	2.761	0.362 18	0.362 02	1.63
12	16	0.362 18	20		2.730	0.366 24		
12	16	0.362 18	20		2.729	0.366 48		
12	16	0.362 18	10	1	2.791	0.358 23	0.358 55	−3.21
12	**16**	**0.362 18**	**2**	**1**	**2.615**	**0.382 36**	**0.381 81**	**5.49**
18	29	0.474 10	10	100	2.113	0.473 33	0.473 10	2.26
18	**29**	**0.474 10**	**2**	**33**	**2.092**	**0.477 95**	**0.477 40**	**5.55**
20	32	0.498 50	10	78	2.018	0.495 57	0.495 15	4.22
20	32	0.498 50	10	44	2.006	0.498 50	0.497 91	5.91
20	32	0.498 50	10	61	1.994	0.501 45	0.501 13	3.22
52	84	0.806 58	10	16	1.243	0.804 78	0.804 70	0.80
52	84	0.806 58	10	27	1.240	0.806 58	0.806 45	1.28
52	84	0.806 58	10	30	1.237	0.808 40	0.808 21	1.89
70	113	0.935 60	10	3	1.073	0.932 09	0.932 05	0.37
70	113	0.935 60	20	9	1.069	0.935 21	0.935 54	−3.31
70	113	0.935 60	10		1.068	0.935 99		
70	113	0.935 60	20	6	1.067	0.937 56	0.937 56	0.00
72	116	0.948 20	10	3	1.061	0.942 03	0.941 80	2.33
72	116	0.948 20	10	2	1.055	0.948 20	0.943 84	43.60
72	116	0.948 20	20	5	1.054	0.948 74	0.948 41	3.33
72	116	0.948 20	20	9	1.053	0.949 75	0.949 85	−0.98
72	116	0.948 20	10	5	1.056	0.946 66	0.946 70	−0.41
72	**116**	**0.948 20**	**2**	**2**	**1.046**	**0.955 91**	**0.955 66**	**2.52**

Table A3. Theoretical and experimental positions of the main reflections for the pentagonal approximant **P2** ($p/q = 7/4$) with the 1D lattice parameter $a = 84.4862$ Å, and tilt angle $\varphi = 3.19°$. This phase of composition $Al_{60}Cu_{30}Fe_{10}$ is obtained after annealing for five days at 709 °C. The phase is icosahedral at 750 °C with the 6D primitive lattice parameter $A = 6.3070$ Å. As in the previous table, rows given in bold type show reflections that belong to the periodic fivefold axis.

N	M	q_{ico} (Å^{-1})	μ	I	d_{theo} (Å)	q_{theo} (Å^{-1})	q_{exp} (Å^{-1})	$\delta q_{(theo-exp)}$ (10^{-4} Å^{-1})
3	**$\bar{1}$**	**0.069 29**	**2**	**1**	**16.898**	**0.059 18**	**0.058 95**	**2.32**
3	$\bar{1}$	0.069 29	10		14.000	0.071 43		
2	1	0.112 11	10	1	9.018	0.110 89	0.110 27	6.21
2	**1**	**0.112 11**	**2**		**8.449**	**0.118 36**		
3	**4**	**0.181 41**	**2**	**1**	**5.633**	**0.177 54**	**0.177 15**	**3.95**
3	4	0.181 41	10	3	5.489	0.182 18	0.181 53	6.47
6	9	0.267 28	10	13	3.748	0.266 77	0.266 82	−0.50
6	9	0.267 28	10	13	3.734	0.267 80	0.270 61	28.10
7	11	0.293 52	10	14	3.412	0.293 04	0.292 79	2.48
7	**11**	**0.293 52**	**2**	**3**	**3.379**	**0.295 91**	**0.295 80**	**1.10**
8	12	0.308 63	10	5	3.259	0.306 81	0.307 23	−4.22
8	12	0.308 63	10	5	3.240	0.308 63	0.308 45	1.80
8	12	0.308 63	10	5	3.221	0.310 45	0.310 16	2.91
18	**29**	**0.474 93**	**2**	**25**	**2.112**	**0.473 45**	**0.473 60**	**−1.47**
18	29	0.474 93	10	100	2.104	0.475 22	0.474 85	3.73
20	32	0.499 37	10	55	2.007	0.498 25	0.498 02	2.27
20	32	0.499 37	10	59	2.002	0.499 37	0.499 10	2.73
20	32	0.499 37	10	55	1.998	0.500 49	0.500 69	−2.03
52	84	0.807 99	10		1.239	0.807 30		
52	84	0.807 99	10	27	1.238	0.807 99	0.807 85	1.38
52	84	0.807 99	10		1.237	0.808 69		
70	113	0.937 23	20		1.068	0.936 48		
70	113	0.937 23	10	8	1.067	0.937 08	0.937 04	0.44
70	113	0.937 23	20		1.067	0.937 38		
70	113	0.937 23	10		1.065	0.938 58		
72	**116**	**0.949 85**	**2**		**1.056**	**0.946 90**		
72	116	0.949 85	10	6	1.052	0.950 44	0.949 57	8.72
72	116	0.949 85	20		1.053	0.949 26		
72	116	0.949 85	20		1.053	0.949 26		
72	116	0.949 85	10	6	1.053	0.949 85	0.949 77	0.83
72	116	0.949 85	10		1.050	0.952 21		

Table A4. Theoretical and experimental positions of the main reflections for the orthorhombic approximant **O** with the 3D lattice parameters $a = 32.1570$ Å, $b = 116.3450$ Å, $c = 19.8510$ Å corresponding to three slightly different 6D primitive lattice parameters $A = B = 6.3102$ Å and $C = 6.3029$ Å. The tilt angles are $\varphi = -1.97^\circ$, $\theta = -0.75^\circ$, and $\gamma = 5.15^\circ$. This phase of composition $Al_{60.3}Cu_{30}Fe_{9.7}$ is obtained after annealing for eight days at 705 °C.

N	M	h	k	l	μ	I	d_{theo} (Å)	q_{theo} (Å^{-1})	q_{exp} (Å^{-1})	$\delta q_{(\text{theo}-\text{exp})}$ (10^{-4} Å^{-1})
6	$\bar{3}$	1	$\bar{3}$	0	4	1	17.671	0.056 59	0.057 15	−5.566
6	$\bar{3}$	0	0	2	4	1	16.079	0.062 19	0.062 04	1.513
6	$\bar{3}$	0	7	1	4		14.765	0.067 73		
6	$\bar{3}$	1	4	1	8		14.608	0.068 46		
3	$\bar{1}$	1	0	1	4	1	16.892	0.059 20	0.059 12	0.798
3	$\bar{1}$	0	4	2	4		14.072	0.071 06		
3	$\bar{1}$	1	7	0	4	1	12.744	0.078 47	0.078 52	−0.530
2	1	1	11	0	4	1	9.334	0.107 13	0.106 86	2.704
2	1	0	7	3	4	1	9.008	0.111 01	0.110 87	1.435
2	1	2	0	2	4	2	8.446	0.118 40	0.118 07	3.281
3	4	3	0	3	4	5	5.631	0.177 60	0.177 42	1.806
3	4	0	11	5	4	2	5.495	0.181 98	0.181 62	3.602
3	4	2	18	0	4	3	5.416	0.184 63	0.184 41	2.118
6	9	0	29	3	4	20	3.757	0.266 15	0.266 05	0.970
6	9	3	18	5	8	7	3.754	0.266 37	0.266 67	−3.019
6	9	2	0	8	4	9	3.726	0.268 41	0.268 08	3.295
6	9	5	11	0	4	4	3.717	0.269 04	0.268 83	2.040
7	11	3	29	0	4	9	3.431	0.291 49	0.291 42	0.764
7	11	0	18	8	4	16	3.413	0.292 96	0.292 88	0.850
7	11	5	0	5	4	12	3.378	0.296 00	0.295 79	2.128
8	12	6	0	0	2	1	3.308	0.302 25	0.302 25	0.000
8	12	3	11	8	8	4	3.267	0.306 05	0.305 87	1.844
8	12	0	36	0	2		3.232	0.309 42		
8	12	5	18	3	8	14	3.226	0.309 97	0.310 31	−3.357
8	12	2	29	5	8		3.220	0.310 58		
8	12	0	0	10	2		3.216	0.310 97		
18	29	8	0	8	4	59	2.111	0.473 61	0.473 72	−1.122
18	29	0	29	13	4	85	2.106	0.474 93	0.474 77	1.624
18	29	5	47	0	4	77	2.101	0.476 06	0.476 29	−2.290
20	32	0	0	16	2	100	2.010	0.497 56	0.498 42	−8.583
20	32	3	47	8	8	98	2.008	0.497 92	0.497 90	0.164
20	32	8	29	5	8	43	2.005	0.498 72	0.499 12	−4.033
20	32	0	58	0	2	78	2.006	0.498 52	0.500 15	−16.356
20	32	5	18	13	8	15	1.997	0.500 81	0.500 76	0.441
20	32	10	0	0	2	7	1.985	0.503 75	0.503 91	−1.548
52	84	16	0	0	2	6	1.241	0.806 00	0.806 65	−6.502
52	84	8	29	21	8	6	1.239	0.806 86	0.807 07	−2.149
52	84	0	94	0	2		1.238	0.807 94		
52	84	13	47	8	8	9	1.237	0.808 67	0.808 70	−0.262
52	84	5	76	13	8	15	1.237	0.808 45	0.808 70	−2.550
52	84	0	0	26	2		1.234	0.810 58		

Table A4. (Continued)

N	M	h	k	l	μ	I	d_{theo} (Å)	q_{theo} (Å^{-1})	q_{exp} (Å^{-1})	$\delta q_{(\mathrm{theo-exp})}$ (10^{-4} Å^{-1})
70	113	16	29	13	8		1.069	0.935 52		
70	113	0	29	29	4		1.069	0.935 64		
70	113	3	76	21	8		1.068	0.935 96		
70	113	8	94	8	8	4	1.068	0.936 52	0.936 33	1.912
70	113	5	105	0	4		1.067	0.936 98		
70	113	13	18	21	8		1.066	0.937 69		
70	113	13	76	21	8		1.066	0.937 95		
70	113	5	47	26	8	6	1.066	0.938 27	0.938 31	−0.352
70	113	18	0	8	4	1	1.063	0.940 26	0.940 51	−2.477
72	116	16	0	16	4		1.056	0.947 21		
72	116	11	76	13	8		1.056	0.947 20		
72	116	16	58	0	4	3	1.055	0.947 71	0.947 70	0.133
72	116	3	105	8	8	2	1.055	0.948 27	0.948 50	−2.249
72	116	0	94	16	4		1.054	0.948 86		
72	116	5	18	29	8		1.054	0.949 04		
72	116	8	65	21	8	4	1.053	0.949 22	0.949 61	−3.966
72	116	0	58	26	4		1.053	0.949 87		
72	116	13	47	18	8	4	1.051	0.951 52	0.951 90	−3.805
72	116	10	94	0	4		1.050	0.952 12		
72	116	18	29	5	8	3	1.049	0.953 16	0.953 34	−1.818
72	116	10	0	26	4		1.050	0.952 63		

References

[1] Tsai A P, Inoue A and Masumoto T 1987 *Japan. J. Appl. Phys.* **26** L1505
[2] Bradley A J and Goldschmidt H J 1939 *J. Inst. Met.* **65** 389
[3] Gayle F W, Shapiro A J, Biancaniello F S and Boettinger W J 1992 *Metall. Trans.* A **23** 2409
[4] Bancel P A 1991 *Quasicrystals: the State of the Art* ed D P DiVicenzo and P J Steinhardt (Singapore: World Scientific) pp 17–55
[5] Faudot F 1993 Les matériaux quasicrystallins *Ann. Chim. Fr.* **18** 445
[6] Audier M and Guyot P 1990 *3rd Int. Mtg on Quasicrystals: Quasicrystals and Incommensurate Structures in Condensed Matter* ed M J Yacaman, D Romeu, V Castano and A Gomez (Singapore: World Scientific) pp 288–99
[7] Audier M and Guyot P 1990 *Proc. Anniversary Adriatico Res. Conf. on Quasicrystals* ed M V Jarić and S Lundqvist (Singapore: World Scientific) pp 74–91
[8] Calvayrac Y, Quivy A, Bessière M, Lefebvre S, Cornier-Quiquandon M and Gratias D 1990 *J. Physique* **51** 417
[9] Gratias D, Calvayrac Y, Devaud-Rzepski J, Faudot F, Harmelin M, Quivy A and Bancel P A 1993 *J. Non-Cryst. Solids* **153&154** 482
[10] Waseda A, Araki K, Kimura K and Ino H 1993 *J. Non-Cryst. Solids* **153&154** 635
[11] Bancel P A 1993 *Phil. Mag. Lett.* **67** 43
[12] Menguy N 1992 *Thesis*
[13] Menguy N, Audier M, Guyot P and Vacher M 1993 *Phil. Mag.* B **68** 595
[14] Menguy N, Audier M, Guyot P and de Boissieu M 1994 *J. Physique Coll. Suppl.* III/IV **4** C3 169
[15] Mayou D, Berger C, Cyrot-Lackmann F, Klein T and Lanco P 1993 *Phys. Rev. Lett.* **70** 3915
[16] Berger C, Mayou D and Cyrot-Lackmann F 1996 *5th Int. Conf. on Quasicrystals* ed C Janot and R Mosseri (Singapore: World Scientific)
[17] Pierce F S, Bancel P A, Biggs B D, Guo Q and Poon S J 1993 *Phys. Rev.* B **47** 5670
[18] Hippert F, Brand R A, Pelloth J and Calvayrac Y 1994 *J. Phys.: Condens. Matter* **6** 11 189
[19] Hippert F, Brand R A, Pelloth J and Calvayrac Y 1996 *5th Int. Conf. on Quasicrystals* ed C Janot and R Mosseri (Singapore: World Scientific)
[20] Gratias D, Katz A and Quiquandon M 1995 *J. Phys.: Condens. Matter.* **7** 9101
[21] Jarić M V and Qiu S Y 1990 *Quasicrystals (12th Taniguchi Symp.)* ed T Fujiwara and T Ogawa (Berlin: Springer) pp 48–56
[22] Cahn J W, Shechtman D and Gratias D 1986 *J. Mater. Res.* **1** 13
[23] Janssen T 1991 *Europhys. Lett.* **14** 131
[24] Yamamoto A and Ishihara K N 1988 *Acta Crystallogr.* A **44** 707
[25] Yamamoto A 1990 *Quasicrystals (12th Taniguchi Symp.)* ed T Fujiwara and T Ogawa (Berlin: Springer) pp 57–67
[26] Saâdi N, Faudot F, Gratias D and Legendre B 1996 *5th Int. Conf. on Quasicrystals* ed C Janot and R Mosseri (Singapore: World Scientific)
[27] Trambly de Laissardière G, Nguyen Manh D, Magaud L, Julien J P, Cyrot-Lackmann F and Mayou D 1995 *Phys. Rev.* B **52** 7920
[28] Bessière M, Quivy A, Lefebvre S, Devaud-Rzepski J and Calvayrac Y 1991 *J. Physique* **1** 1823
[29] Katz A and Gratias D 1993 *J. Non-Cryst. Solids* **153&154** 187